

# Analytical approximations for spiral waves

Jakob Löber<sup>1, a)</sup> and Harald Engel<sup>1</sup>

*Institut für Theoretische Physik, Technische Universität Berlin, Hardenbergstrasse 36, 10623 Berlin, Germany*

We propose a non-perturbative attempt to solve the kinematic equations for spiral waves in excitable media. From the eikonal equation for the wave front we derive an implicit analytical relation between rotation frequency  $\Omega$  and core radius  $R_0$ . For free, rigidly rotating spiral waves our analytical prediction is in good agreement with numerical solutions of the linear eikonal equation not only for very large but also for intermediate and small values of the core radius. An equivalent  $\Omega(R_+)$  dependence improves the result by Keener and Tyson for spiral waves pinned to a circular defect with radius  $R_+$  with Neumann boundaries at the periphery. Simultaneously, analytical approximations for the shape of free and pinned spirals are given. We discuss the reasons why the ansatz fails to correctly describe the result for the dependence of the rotation frequency on the excitability of the medium.

PACS numbers: 82.40.Bj, 05.45.-a, 05.65.+b, 47.54.-r

Keywords: spiral waves, frequency selection, free boundary

## I. INTRODUCTION

Spiral waves are a common occurrence in excitable media. They have been observed in systems as diverse as catalytic surface reactions<sup>1</sup>, the Belousov-Zhabotinsky chemical reactions<sup>2,3</sup> and social amoeba colonies<sup>4</sup>. They play an important role as pathological states of action potential propagation in cardiac tissue and are thought to be the precursor of ventricular fibrillation<sup>5</sup>.

In the simplest case, a free spiral rotates rigidly with a frequency  $\omega$  while its tip describes a circular trajectory with radius  $r_0$ , called the spiral core radius. From experiments and numerical simulations it is well-known that spiral waves select their own, unique asymptotic wave shape and rotation frequency. Thus, independently on the method of initiation, coexisting (and non-interacting) spiral waves in a spatially uniform excitable or oscillatory medium exhibit the same wave length, core radius and rotation frequency after all transients have died out. Exceptions to this rule are known only for media with anomalous dispersion of periodic wave trains<sup>6</sup>.

A theoretical description aims to understand the underlying selection principle determining shape, rotation frequency and core radius of spiral waves. One successful approach is the free boundary or kinematic approach<sup>7,8</sup> which reduces the nonlinear reaction-diffusion equations to simpler equations describing the motion of interfaces separating excited from resting states. In contrast to earlier works, which mapped wave front and wave back onto each other<sup>7,9,10</sup>, it became clear that one has to solve equations for both the front and back interface of a spiral to yield a self-consistent solution for  $\omega$  and  $r_0$ .

Within the free-boundary approach, the pattern selection problem for wave segments<sup>11</sup>, which are unstable solutions of the reaction-diffusion system, has been solved. These patterns undergo translational motion in

an unbounded medium. The properties of the medium were expressed by a single dimensionless parameter  $B$  that can be interpreted as a measure of the local excitation threshold which increases with  $B$  while the excitability decreases. Wave segments exist in a finite range  $0 \leq B \leq B_c$  of  $B$ -values.

In the limit  $B \rightarrow 0$ , wave segments correspond to motionless circular spots<sup>12</sup>. At the upper boundary of the existence range, for  $B \rightarrow B_c \approx 0.535$ , they merge with spiral waves in a separatrix solution known as the critical finger<sup>13</sup>. The critical finger is an half-infinite plane pulse with an open end that can be regarded as a spiral wave rotating with zero frequency around an infinitely large core.

Spiral waves with  $B \lesssim B_c$  close to the critical finger and their transition into meandering spiral waves were analytically investigated by Hakim and Karma<sup>14</sup> applying methods of singular perturbation theory. For  $B > B_c$ , only retracting fingers were found to exist because the excitability of the system is too weak to support wave segments and spiral waves. The entire range  $B_{\min} \leq B \leq B_c$  for which spiral waves coexist with wave segments as a solution to the kinematic equations was studied numerically by Zykov in<sup>15,16</sup>. For  $B \rightarrow B_{\min} \approx 0.211$  the spiral core radius  $r_0$  decreases to zero and for  $B < B_{\min}$ , rigidly rotating spiral waves cease to exist.

Solving the kinematic equations in a disk with a Neumann boundary led to the discovery of boundary spots. Boundary spots are unstable wave solutions to reaction-diffusion equations that rotate at a lower frequency than spiral waves. Furthermore, in contrast to spiral waves, boundary spots do not extend over the entire disk but remain spatially localized close to the disc boundary<sup>17</sup>.

In this work, we follow an analytical non-perturbative approach that goes back to a classical paper by Burton, Cabrera and Frank<sup>18</sup>. Their approach is non-perturbative in the sense that it does not rely on a small parameter for a perturbation expansion. These authors considered spiral waves occurring in crystal growth which

<sup>a)</sup>Electronic mail: jakob@physik.tu-berlin.de

have a vanishing core radius. They used an ansatz function for the wave shape to calculate the rotation frequency of spirals. Keener<sup>19</sup> and Tyson and Keener<sup>8</sup> extended this ansatz to spirals pinned to a circular hole with finite core radius with a no-flux boundary condition at the periphery. In this case the selection problem turns out to be much simpler than for free spiral waves because the rotation frequency can be determined from the equation for the front interface alone while the core radius is given by the radius of the Neumann hole.

Below, we present a non-perturbative approach which does not only improve the result obtained by Keener and Tyson for pinned spiral waves, but also works quite well for free spirals. In Sec. II, we state the equations of the free-boundary approach and review existing solutions. Our ansatz is introduced in Sec. III. The analytical results for free and pinned spirals are presented in Sec. IV and Sec. V, respectively, and compared to numerical solutions of the kinematic equations. We end with discussion of the results, conclusion and outlook in Sec. VI.

## II. KINEMATIC EQUATIONS

We consider a standard activator ( $u$ ) -inhibitor ( $v$ ) reaction-diffusion systems of the form

$$\partial_t u = \epsilon \nabla^2 u + f(u, v) / \epsilon, \quad (1)$$

$$\partial_t v = g(u, v), \quad (2)$$

where the dimensionless parameter  $0 < \epsilon \ll 1$  is a measure for the time scale separation between activator and inhibitor and serves as a small parameter for a perturbation expansion. We neglect inhibitor diffusion and scale space accordingly so that the activator diffusion coefficient is equal to  $\epsilon$ . The  $u$  nullcline obtained from  $f(u, v) = 0$  is assumed to be  $S$ -shaped in the  $(u, v)$  plane. A simple choice for the functions  $f$  and  $g$  is given by the FitzHugh-Nagumo kinetics

$$f(u, v) = 3u - u^3 - v, \quad (3)$$

$$g(u, v) = u - \delta, \quad (4)$$

with a unique, linearly stable rest state  $u_0 = \delta$ ,  $v_0 = 3\delta - \delta^3$ .

If  $\epsilon$  is small, a traveling pulse can be regarded as consisting of two separate spatial regions: an excited region ( $\mathcal{D}^+$ ), where the value of the activator is large and the inhibitor is rising, and a refractory region ( $\mathcal{D}^-$ ), where the activator value is small and the inhibitor is decaying. This behavior is described by the outer equations Eqs. (1), (2), which in lowest order to  $\epsilon$  read<sup>8</sup>

$$0 = f(u^\pm(v), v), \quad (5)$$

$$\partial_t v = g(u^\pm(v), v) \text{ in } \mathcal{D}^\pm. \quad (6)$$

Here,  $u^+(v)$  and  $u^-(v)$  denote the largest respectively smallest root of  $f(u, v) = 0$  which the activator follows

in the excited respectively refractory region. The two regions  $\mathcal{D}^+$  and  $\mathcal{D}^-$  are separated by a front (+) and a back (-) interface, where the activator value changes very fast from a low to a high value and the other way round, respectively. These interfaces can be regarded as fronts traveling with velocities  $c^\pm$ . They are solutions to the inner equations, obtained from Eqs. (1), (2) by a change of scale in time and space proportional to  $\epsilon$ . The expression for the front velocity together with Eq. (6) and appropriate periodic boundary conditions yield the dispersion relation for a periodic pulse train, i.e., the dependence of the propagation velocity  $c$  on the period length  $L$  to lowest order in  $\epsilon$ <sup>8,19</sup>.

In two spatial dimensions, the shape of the front (+) and back (-) interfaces for rigidly rotating spiral waves are conveniently parametrized by  $\theta^\pm(r)$  using polar coordinates

$$\begin{pmatrix} x^\pm(r, t) \\ y^\pm(r, t) \end{pmatrix} = \begin{pmatrix} r \cos(\theta^\pm(r) - \omega t) \\ r \sin(\theta^\pm(r) - \omega t) \end{pmatrix}. \quad (7)$$

In Eq. (7),  $\omega > 0$  is the rotation frequency of a spiral wave rotating counterclockwise. The inner equations in two spatial dimensions provide a relation between the normal velocity  $c_n^\pm$  of the moving front and back interface and its local curvature  $\kappa^{\pm 19}$ , the so-called linear eikonal equation

$$c_n^\pm(r) = c^\pm(v^\pm) - \epsilon \kappa^\pm(r). \quad (8)$$

Here  $v^\pm$  denote the inhibitor level at the interface, and  $c^\pm(v^\pm)$  is the velocity of a planar front moving through a medium with a constant inhibitor value  $v^\pm$ . Similar as for a one-dimensional pulse train, Eq. (6) yields together with the condition of periodicity in  $\theta$  an expression for  $c^\pm(v^\pm)$ . This constitutes the so-called wave front interaction model. The interaction between wave front and wave back is mediated through the dependence of  $v^+$  and  $v^-$  on the positions of both front and back interface. With the chosen parametrization, the curvature  $\kappa^\pm$  is expressed as

$$\kappa^\pm(r) = -\frac{\theta^{\pm'}(r)}{\left(1 + (r\theta^{\pm'}(r))^2\right)^{1/2}} - \frac{(d/dr)(r\theta^{\pm'}(r))}{\left(1 + (r\theta^{\pm'}(r))^2\right)^{3/2}}, \quad (9)$$

and the normal velocity is given by

$$c_n^\pm(r) = \frac{r\omega}{\left(1 + (r\theta^{\pm'}(r))^2\right)^{1/2}}. \quad (10)$$

Eq. (8) has to be supplemented with appropriate boundary conditions. For a rigidly rotating free spiral wave, front and back interface meet continuously at the apex  $r = r_0$  of the spiral, i.e.,

$$\theta^\pm(r_0) = 0, \quad (11)$$

where we fixed an arbitrary initial phase of the spiral to be zero. The apex is the point of closest approach of both

interfaces to the center of rotation (compare Fig. 1). At the apex, the normal velocity is zero,  $c_n^\pm(r_0) = 0$ . Both interfaces approach the apex tangentially to a circle with core radius  $r_0$ , so that

$$\theta^{+'}(r_0) = -\theta^{-'}(r_0) = \infty. \quad (12)$$

This circle is considered as the spiral core with  $r_0$  being the core radius.

Far from the core, front and back interface behave as an Archimedean spiral,

$$\theta^\pm(r) \sim r, \quad (r \rightarrow \infty). \quad (13)$$

Eqs. (11), (12), (13) fix six boundary conditions for two coupled second order ordinary differential equations (ODEs) Eq. (8). Four boundary conditions are necessary to determine the four integration constants of these ODEs. The remaining two are used to determine two unknown nonlinear eigenvalues introduced as parameters in the eikonal equation and the boundary conditions: the rotation frequency  $\omega$  and the spiral core radius  $r_0$ . The full wave front interaction model, as given by Eq. (6) together with the linear eikonal equation Eq. (8) was solved numerically by Pelcé and Sun in<sup>20</sup> without any further approximations for a piecewise linear activator kinetics. Because Eq. (6) is too difficult for an analytical treatment, further approximations are necessary. Assuming that the inhibitor value  $v$  stays always close to the stall level  $v = v_s$  given by  $c^\pm(v_s) = 0$ , Eq. (6) can be simplified<sup>14</sup>

$$\partial_t v = \frac{1}{\tau_e} \text{ in } \mathcal{D}^+, \quad (14)$$

$$\partial_t v = -\frac{v - v_0}{\tau_R} \text{ in } \mathcal{D}^-, \quad (15)$$

$$c^\pm(v^\pm) = \alpha(v_s - v^\pm), \quad (16)$$

with the abbreviations

$$\tau_e = \frac{1}{g(u^+(v_s), v_s)}, \quad (17)$$

$$\tau_R = \frac{\partial_u f}{\partial_u g \partial_v f - \partial_v g \partial_u f} \Big|_{u=u^-(v_s), v=v_s}. \quad (18)$$

This approximation assumes a linear rise of the inhibitor during the excited period on a time scale of the order  $\tau_e$ , followed by an exponential decay during the refractory period on the time scale  $\tau_R$ .

Spiral waves close to the critical finger have a diverging period, so that the inhibitor value  $v^+$  has already decayed to its rest value,  $v^+ = v_0$ , everywhere along the front interface. In this case,  $v^-$  determined by Eqs. (14), (15) depends linearly on the angular pulse width  $\Delta\theta(r) = \theta^+(r) - \theta^-(r)$ , and the expressions for  $c^\pm$  become particularly simple

$$c^+(v^+) = c, \quad (19)$$

$$c^-(v^-) = -c + \frac{b}{\omega} (\theta^+(r) - \theta^-(r)). \quad (20)$$

$c = \alpha(v_s - v_0) > 0$  corresponds to the velocity of a front solution of the inner equations moving through a medium with a constant inhibitor at its rest state  $v = v_0$ . Note that the eikonal equation for the front interface decouples from the equation for the back, while the back interface interacts with the front interface via a term that is linear in the pulse width. The single kinetic parameter  $b = \alpha/\tau_e > 0$  is a measure for the strength of this interaction. For FitzHugh-Nagumo kinetics according to Eqs. (3), (4), we find  $\alpha = 1/\sqrt{2}$ ,  $v_s = 0$ ,  $\tau_e = \frac{1}{\sqrt{3-\delta}}$  and  $\tau_R = 6$ .

Hakim and Karma<sup>14</sup> used singular perturbation theory to expand the eikonal equation Eq. (8) around the critical finger. In that way, they obtain analytical expressions for spiral waves with a very large core radius. We review their approach in the following. Taking into account Eqs. (19), (20), the eikonal equations for front and back are

$$c_n^+(r) = c - \epsilon \kappa^+(r), \quad (21)$$

$$c_n^-(r) = \frac{b}{\omega} (\theta^+(r) - \theta^-(r)) - c - \epsilon \kappa^-(r). \quad (22)$$

Similar as in the derivation of the eikonal equations from the reaction diffusion system,  $\epsilon$  serves as the small parameter for a singular perturbation expansion. For both the front and back interface three scaling regions were identified: the spiral tip region near to the core, an intermediate region, and one region sufficiently far from the core where curvature effects are less important. The outer equations valid in the region far from the core are Eqs. (21), (22) with  $\epsilon = 0$ . Its solution

$$\psi_{\text{inv}}^+(r) = r\theta_{\text{inv}}^{+'}(r) = -\sqrt{\frac{r^2\omega^2}{c^2} - 1}, \quad (23)$$

$$\theta_{\text{inv}}^-(r) = \theta_{\text{inv}}^+(r) - \frac{2c\omega}{b}, \quad (24)$$

describes the involute of a circle of radius  $r_0$  which asymptotically transforms into an Archimedean spiral for  $r \rightarrow \infty$ .

The behavior in the tip region is described by the equations for the critical finger. While the equation for the front can be solved analytically<sup>11</sup>, no analytical solution is known for the back. Matching the analytical solutions for the front interface in the tip, intermediate and far core regions, Hakim and Karma succeeded to derive analytically a relationship between rotation frequency  $\omega$  and core radius  $r_0$ . Matching the solutions for the back interface and using stability arguments, an expression for the core radius  $r_0$  involving two numerically determined constants was obtained. Together, these two relations yield the desired dependence of the spiral wave frequency  $\omega$  on the kinetic parameter  $b$ . It should be emphasized that these solutions are only valid for small  $\epsilon$  and for spiral waves close to the critical finger which have a diverging core radius.

The eikonal equations for wave front and back, Eqs. (21), (22), can be rescaled by introducing dimensionless quan-

tities according to

$$r_0 = \frac{R_0 \epsilon}{c}, \quad r = \frac{R \epsilon}{c}, \quad \omega = \frac{c^2 \Omega}{\epsilon}, \quad b = \frac{B c^3}{\epsilon}, \quad c_n^\pm = c C_n^\pm, \quad (25)$$

and rescaled shape functions  $\Theta^\pm$  as

$$\theta^\pm(r) = \theta^\pm\left(\frac{R \epsilon}{c}\right) = \Theta^\pm(R) \quad (26)$$

and

$$\Psi^\pm(R) = R \Theta^{\pm'}(R). \quad (27)$$

Here we introduced the dimensionless parameter  $B$  as a measure of the excitation threshold. The rescaling of  $b$  by  $\epsilon$  is justified close to the critical finger because there  $B \rightarrow B_c \approx 0.535$  is of order one. In the following all rescaled dimensionless quantities will be denoted by upper case letters, while lower case letters are used for dimensional quantities. In dimensionless terms Eq. (21) and Eq. (22) read

$$C_n^+(R) = 1 - K^+(R), \quad (28)$$

$$C_n^-(R) = -1 + \frac{B}{\Omega} (\Theta^+(R) - \Theta^-(R)) - K^-(R). \quad (29)$$

Note that the small parameter  $\epsilon$  as well as the propagation velocity  $c$  in the eikonal equations have been eliminated under the rescaling.

Strictly speaking, these rescaled eikonal equations can only be valid in the limit of spirals with diverging core radius. The front interface of spiral waves with finite core radius  $R_0$  interacts with the back interface of the wave ahead because it does not propagate into a fully recovered medium. In general, the front inhibitor level  $v^+$  depends on the radial coordinate  $r$ . Zykov<sup>16</sup> introduces a further approximation: assuming a constant value  $v^+$  of the inhibitor at the front interface, with  $v^+$  given by the dispersion relation of a one-dimensional periodic pulse train, and using a slightly different rescaling, the dimensionless eikonal equations Eqs. (28), (29) can be also be used for spirals which are not close to the critical finger. Applying a numerical shooting method, Zykov<sup>15,16</sup> then proceeds to demonstrate the existence of spiral wave solutions to these equations in a certain interval  $B_{\min} \approx 0.211 < B \lesssim B_c \approx 0.535$  of the dimensionless excitability parameter  $B$  and determined a universal relationship  $\Omega(B)$ . At  $B = B_{\min} \approx 0.211$  the shape of the front interface is identical to that obtained by Burton, Cabrera and Frank (BCF)<sup>18</sup> for a spiral wave with zero core radius rotating at frequency  $\Omega \approx 0.331$ . The back interface results from turning the front interface clockwise around an angle  $\Delta\Theta(R) = \Theta^+(R) - \Theta^-(R) = \pi$ . In the other limit, for  $B \lesssim B_c \approx 0.535$ , the analytical results of Hakim and Karma for spirals with diverging core radius are recovered. The numerically obtained universal relationship  $\Omega(B)$  together with the dispersion relation

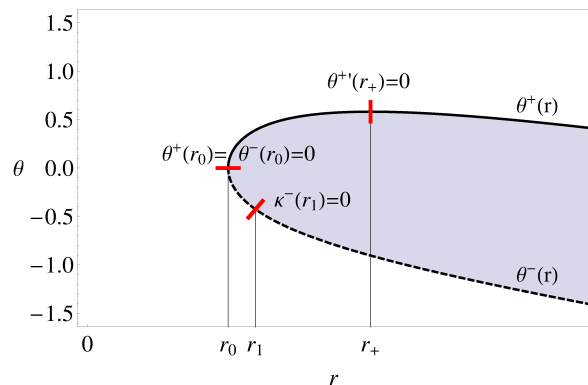


Figure 1. Close-up of the spiral tip region. Front ( $\theta^+(r)$ , solid line) and back ( $\theta^-(r)$ , dashed line) interface separate the shaded excited region  $\mathcal{D}^+$  from the white refractory region  $\mathcal{D}^-$ . At the core radius  $r_0$ , the point  $r_+$  at the wave front and the inflection point  $r_1$  at the wave back, approximate and exact analytical solution of the free-boundary problem have the same leading order asymptotic expansions.

of one dimensional pulse trains is sufficient to predict the rotation frequency of rigidly rotating spiral waves. Though only approximately valid, this approach clearly separates the two physical mechanisms underlying the frequency selection for spiral waves:

I. The interaction of the front interface with the back interface of the preceding wave essentially leads to a front moving through a partially recovered medium. This in turn leads to a slower velocity of the front as approximately given by the dispersion relation of a one-dimensional periodic pulse train.

II. The interaction of the back interface with the front interface within the same wave is proportional to the angular pulse width  $\Delta\Theta(R) = \Theta^+(R) - \Theta^-(R)$  and characterized in strength by the dimensionless parameter  $B$ .

That the kinetic characteristics of the medium can be lumped together into a single parameter  $B$  simplifies the determination of the parameter range of spiral wave existence significantly.

Front and back interface of spiral waves pinned to a circular Neumann hole of radius  $r_+$  approach the hole in radial direction, so that  $\theta^\pm$  fulfills the boundary condition

$$\theta^{\pm'}(r_+) = 0. \quad (30)$$

which implies that the spiral arm is orthogonal to the hole. Note that a corresponding point  $r = r_+$  can always be found at the front interface of a freely rotating spiral wave, see Fig. 1. The kinematic equation for the front interface of a pinned spiral wave was studied analytically by Keener and Tyson<sup>8,19</sup>. These authors determined the asymptotic behavior of solutions to Eq. (21) for the front interface as  $r \rightarrow r_+$  and  $r \rightarrow \infty$ . An ansatz showing the same asymptotic behavior and involving several con-

stants was used. Comparing the asymptotics of ansatz and solution, they were able to determine the constants of the ansatz and finally derived a relation between rotation frequency  $\omega$  and hole radius  $r_+$ .

### III. ASYMPTOTES TO SOLUTIONS AND ANSATZ

In this section, we propose an attempt to solve the kinematic Eqs. (21), (22) together with the boundary conditions for a free spiral wave Eqs. (11), (12), and (13). First, we obtain asymptotes to the solutions to these linear eikonal equations. Asymptotes to the solutions for the front and back interface can be obtained at the spiral core,  $r \rightarrow r_0$ , and very far from the core as  $r \rightarrow \infty$ . Additionally, an asymptote can be obtained at the point  $r \rightarrow r_+$  of the front interface. Furthermore, the existence of an inflection point at  $r = r_1$  at the back interface is taken into account. Second, we present an ansatz for the interface shape  $\theta^\pm(r)$  that reproduces in leading order all these asymptotic expansions correctly. See e. g.<sup>21</sup> how to compute asymptotes to solutions to differential equations.

#### A. Asymptotes to solutions to the linear eikonal equation

Far from the core the shape of the interfaces is asymptotically Archimedean, i.e.,

$$\theta^\pm(r) = -\frac{\omega}{c}r + \mathcal{O}(\log(r)), \quad r \rightarrow \infty. \quad (31)$$

At the spiral core, the asymptotic behavior that fulfills the two boundary conditions Eqs. (11), (12) is given by

$$\theta^\pm(r) = \pm \frac{\sqrt{2\epsilon}}{\sqrt{cr_0^2 + \epsilon r_0}} \sqrt{r - r_0} + \mathcal{O}(r - r_0), \quad r \rightarrow r_0. \quad (32)$$

Finally, at the distance  $r = r_+$  (compare Fig. 1), an asymptotic expansion for the front interface is available which reads<sup>8,19</sup>

$$\theta^{+\prime}(r) = \frac{(r_+\omega - c)}{r_+\epsilon} (r - r_+) + \mathcal{O}\left((r - r_+)^2\right), \quad r \rightarrow r_+. \quad (33)$$

The back interface of spiral waves always exhibits an inflection point at  $r = r_1$  where the curvature  $\kappa^-$  vanishes

$$\kappa^-(r_1) = 0. \quad (34)$$

In polar coordinates the inflection point is not easy visible, see Fig. 1, while it appears clearly pronounced in Cartesian coordinates used in Fig. 4. From the eikonal equation for the back Eq. (22) follows at the inflection point

$$c_n^-(r_1) = c^-(r_1), \quad (35)$$

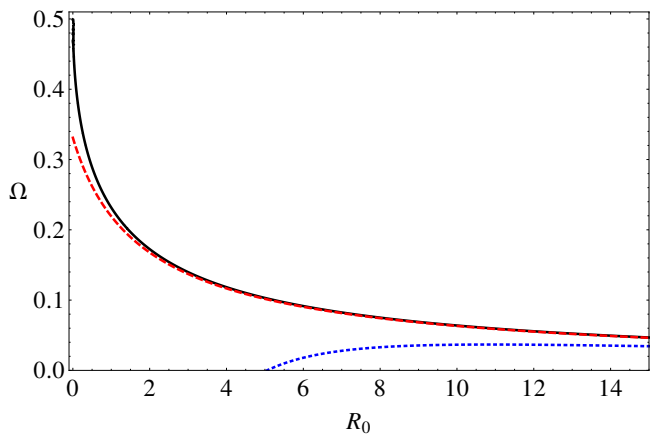


Figure 2. Dimensionless rotation frequency  $\Omega$  over dimensionless spiral core radius  $R_0$  for rigidly rotating spiral waves. The analytically obtained result according to Eq. (46) (black solid line) is compared to numerical solutions of the linear eikonal equations Eqs. (28), (29) (red dashed line). The blue dotted line shows the analytical result for diverging core radius<sup>14</sup>.

which using Eq. (10) leads to the following expression for the parameter  $b$

$$b = \frac{\omega}{\theta^+(r_1) - \theta^-(r_1)} \left( c + \frac{r_1\omega}{\sqrt{(r_1\theta^{-\prime}(r_1))^2 + 1}} \right). \quad (36)$$

Note that although we present here the asymptotes to solutions of the unscaled eikonal equations, Eqs. (21), (22), a rescaling according to Eq. (25) yields the corresponding asymptotes of the rescaled eikonal equations Eqs. (28), (29). As it should be the case,  $\epsilon$  and  $c$  drop out under this rescaling in every expression for the asymptotes.

#### B. Asymptotic behavior of the ansatz

We use the ansatz

$$\psi_{\text{ans}}^\pm(r) = r\theta_{\text{ans}}^{\pm\prime}(r) = A_\pm \frac{r^2 - r_\pm^2}{\sqrt{r^2 - r_0^2}}, \quad (37)$$

which yields for the interface shape  $\theta_{\text{ans}}^\pm(r)$

$$\begin{aligned} \theta_{\text{ans}}^\pm(r) &= \int_{r_0}^r d\tilde{r} \frac{\psi_{\text{ans}}^\pm(\tilde{r})}{\tilde{r}} \\ &= A_\pm \left( \sqrt{r^2 - r_0^2} - \frac{r_\pm^2}{r_0} \arccos\left(\frac{r_0}{r}\right) \right). \end{aligned} \quad (38)$$

Such an ansatz can only be justified by virtue of the validity of the conclusions derived from it. It involves five constants  $A_\pm$ ,  $r_\pm$  and  $r_0$ . For  $r_- \leq r_0$ , the back interface described by  $\theta_{\text{ans}}^-$  exhibits an inflection point at a point  $r_1 \geq r_0$ . Thus, valid solutions for the front and back of a free spiral can only be found if

$$r_+ \geq r_0 \geq r_- \geq 0. \quad (39)$$

So in contrast to the spiral core radius  $r_0$  and the corresponding Neumann hole radius  $r_+$ ,  $r_-$  does not have a direct physical interpretation. All five constants together with the spiral wave frequency  $\omega$  are determined by comparing the asymptotics of the ansatz with the asymptotes to the solution to the eikonal equations. Our ansatz produces the correct leading order asymptotics for  $r \rightarrow \infty$

$$\theta_{\text{ans}}^{\pm}(r) = A_{\pm}r + \mathcal{O}(1), \quad r \rightarrow \infty, \quad (40)$$

and for  $r \rightarrow r_0$

$$\begin{aligned} \theta_{\text{ans}}^{\pm}(r) &= A_{\pm} \frac{\sqrt{2}}{r_0^{3/2}} (r_0^2 - r_{\pm}^2) \sqrt{r - r_0} \\ &\quad + \mathcal{O}\left((r - r_0)^{3/2}\right), \quad r \rightarrow r_0. \end{aligned} \quad (41)$$

At the point  $r = r_+$ , the ansatz for the front interface displays the asymptotic behavior corresponding to a Neumann boundary

$$\theta_{\text{ans}}^{+ \prime}(r) = \frac{2A_+}{\sqrt{r_+^2 - r_0^2}} (r - r_+) + \mathcal{O}\left((r - r_+)^2\right), \quad r \rightarrow r_+. \quad (42)$$

The sixth relation is the inflection point at  $r = r_1$  with a vanishing curvature at the spiral wave back, Eq. (34). Equating the six asymptotic expansions of the ansatz with the six asymptotes to the solutions to the linear eikonal equation, we are able to determine four unknown parameters  $A_{\pm}$  and  $r_{\pm}$ , as well as the relations  $\omega$  over  $r_0$  and  $r_0$  over  $b$ .

#### IV. RESULTS FOR FREE SPIRALS

##### A. Rotation frequency $\Omega$ versus core radius $R_0$

Comparing Eq. (32) with Eq. (40), and Eq. (31) with Eq. (41), we get

$$A_{\pm} = -\frac{\omega}{c}, \quad (43)$$

$$r_{\pm} = \sqrt{r_0 \left( r_0 \pm \frac{c}{\omega} \sqrt{\frac{\epsilon}{cr_0 + \epsilon}} \right)}. \quad (44)$$

Equating the asymptotic expressions for  $r \rightarrow r_+$  given by Eqs. (42) and (33) we obtain an implicit relation between frequency  $\omega$  and core radius  $r_0$

$$\omega = \sqrt{\frac{c^2 \omega}{cr_0 \sqrt{\frac{\epsilon}{cr_0 + \epsilon}} + r_0^2 \omega}} - 2 \sqrt{\frac{\omega^3 \sqrt{\epsilon^3 (cr_0 + \epsilon)}}{c^3 r_0}}. \quad (45)$$

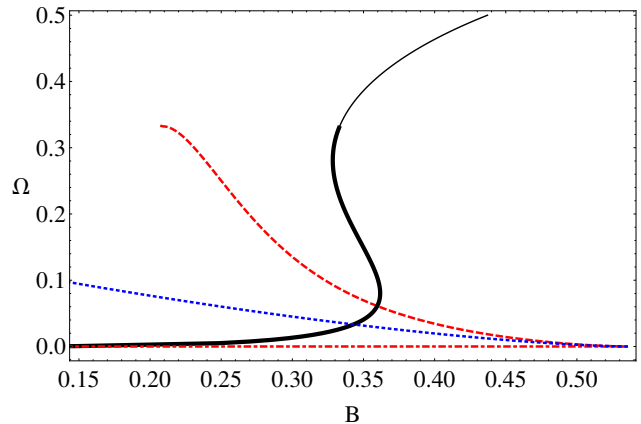


Figure 3. Rotation frequency  $\Omega$  versus excitability parameter  $B$  in dimensionless units. The red dashed and dash-dotted lines represent the branches of spiral waves respectively wave segments obtained numerically from the linear eikonal equations Eqs. (28), (29). The two branches merge for  $B = B_c \approx 0.535$  (critical finger<sup>13</sup>). The analytical approximation is shown by the black solid line where the thick segment corresponds to the frequencies below  $\Omega = \Omega_{\text{BCF}} \approx 0.331$  (Burton-Cabrera-Frank limit). The blue dotted line shows the analytical result from<sup>14</sup>.

In rescaled form, Eq. (45) reads

$$\sqrt{R_0} \Omega = \sqrt{\frac{\sqrt{R_0 + 1} \Omega}{1 + R_0 \sqrt{R_0 + 1} \Omega}} - 2 \sqrt{\Omega^3 \sqrt{R_0 + 1}}. \quad (46)$$

The last expression can be written as

$$\tilde{\Omega} \left( 1 + \tilde{\Omega} \right) \left( R_0 + 2\sqrt{\tilde{\Omega}} \right)^2 - R_0^2 (1 + R_0) = 0 \quad (47)$$

where we have introduced the abbreviation

$$\tilde{\Omega} = R_0 \sqrt{1 + R_0} \Omega \quad (48)$$

which can be used to rewrite  $R_{\pm}$  from Eq. (44) in the form

$$R_{\pm} = \sqrt{R_0 \left( R_0 \pm \frac{1}{\sqrt{1 + R_0} \Omega} \right)} = R_0 \sqrt{1 \pm \frac{1}{\tilde{\Omega}}}. \quad (49)$$

From Descartes rule of signs we conclude that the number of positive real roots of the sextic polynomial Eq. (47) is one. Thus,  $\Omega$  over  $R_0$  has only one physically meaningful branch.

Unfortunately, it is not possible to determine an explicit relation for  $\Omega(R_0)$  from Eq. (46) or Eq. (47). However, we can determine the asymptotic behavior of  $\Omega(R_0)$  for large and small core radii  $R_0$  as

$$\Omega = \frac{1}{2} - \frac{1}{2\sqrt{2}} \sqrt{R_0} + o\left(\sqrt{R_0}\right), \quad R_0 \rightarrow 0 \quad (50)$$

and

$$\Omega = \frac{1}{R_0} - \frac{1}{2R_0^{3/2}} + \mathcal{O}\left(R_0^{-7/4}\right), \quad R_0 \rightarrow \infty. \quad (51)$$

Thus, we obtain a finite rotation frequency for vanishing core radius. However, with  $\Omega(R_0 \rightarrow 0) = 1/2$  we miss the Burton-Cabrera-Frank limit  $\Omega \approx 0.331$ .

Our theoretical prediction for  $\Omega(R_0)$  matches well with direct numerical solutions of the rescaled eikonal equations Eqs. (28), (29) (compare black solid respectively red dashed line Fig. 2) where in particular the good agreement for intermediate and even quite small core radii is remarkable.

Hakim and Karma found with singular perturbation theory for the case of very large core radius  $r_0$  and small  $\epsilon^{14}$

$$\omega_{\text{HK}}(r_0) = \frac{c}{r_0} + 2^{1/3} \frac{a_1}{r_0^{5/3}} \epsilon^{2/3}, \quad (52)$$

which in rescaled form reads

$$\Omega_{\text{HK}}(R_0) = \frac{1}{R_0} + 2^{1/3} \frac{a_1}{R_0^{5/3}}, \quad (53)$$

where  $a_1 = -2.3381$  denotes the first zero of the Airy function  $\text{Ai}(x)$ . The dependence Eq. (53) corresponds to the blue dotted line in Fig. 2. To compare our result with the result by Hakim and Karma, we can expand our result Eq. (45) for small  $\epsilon$ ,

$$\omega(r_0) = \frac{c}{r_0} - \frac{c^{1/2}}{2r_0^{3/2}} \epsilon^{1/2} + \mathcal{O}(\epsilon^{3/4}). \quad (54)$$

Note the different exponents in  $\epsilon$  and  $r_0$ .

Another justification of our ansatz is given by the following observation. For  $\epsilon = 0$ , Eq. (44) and (45) reduce to

$$\omega = \frac{c}{r_0}, \quad (55)$$

$$r_+ = r_0, \quad (56)$$

i.e., our ansatz reduces to the involute spiral

$$\lim_{\epsilon \rightarrow 0} \psi_{\text{ans}}^+(r) = -\sqrt{\frac{r^2}{r_0^2} - 1}. \quad (57)$$

Eq. (57) gives the correct solution of the linear eikonal equation for the front interface for  $\epsilon = 0$ , compare Eq. (23).

## B. Rotation frequency $\Omega$ as a function of $B$

Upon rescaling (36) and comparing it with the ansatz, we can express  $B$  in the form

$$B = \frac{\Omega + \frac{R_1 \Omega^2}{\sqrt{R_1^2 (\Theta_{\text{ans}}^-(R_1))^2 + 1}}}{\Theta_{\text{ans}}^+(R_1) - \Theta_{\text{ans}}^-(R_1)}. \quad (58)$$

Here,  $R_1$  is given by

$$K^-(R_1) = 0 \quad (59)$$

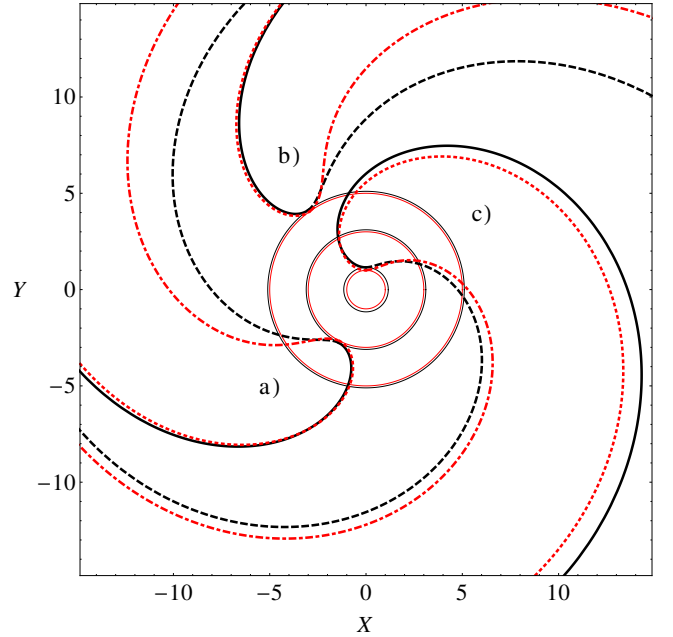


Figure 4. Front and back interface of free spiral waves in the core region. Black solid and dashed lines show analytical approximations for wave front respectively back as obtained from Eq. (66) using  $\Omega(R_0)$  given by Eq. (46). Red dotted and dot-dashed lines are plots of the corresponding numerical results. The rotation frequency was fixed to a)  $\Omega = 0.137$ , b)  $\Omega = 0.102$ , c)  $\Omega = 0.219$ . The analytically obtained core radii (black circles) are a)  $R_0 = 3$ , b)  $R_0 = 5$ , c)  $R_0 = 1$ .

or explicitly

$$R_1^2 \Theta_{\text{ans}}^-(R_1)^3 + R_1 \Theta_{\text{ans}}^{\prime\prime}(R_1) + 2 \Theta_{\text{ans}}^{\prime}(R_1) = 0. \quad (60)$$

If we numerically solve the algebraic Eqs. (58) and (60) together with the ansatz Eq. (38) and use the relation for  $\Omega$  over  $R_0$  Eq. (46), we obtain the dependence  $\Omega(B)$  plotted as black solid line in Fig. 3. Analytically we can determine  $B$  as a function of  $\Omega$  in the limit  $\Omega \rightarrow \frac{1}{2}$  corresponding to  $R_0 \rightarrow 0$

$$\lim_{\Omega \rightarrow \frac{1}{2}} B(\Omega) = \frac{1}{4 \text{arcsec}(2^{1/4})} \approx 0.437171, \quad (61)$$

and in the limit  $\Omega \rightarrow 0$  corresponding to  $R_0 \rightarrow \infty$

$$\lim_{\Omega \rightarrow 0} B(\Omega) = 0. \quad (62)$$

From the obtained  $\Omega(B)$  dependence we conclude that spiral wave solutions to the linear eikonal equation exist within this finite range of  $B$  values. However, our ansatz clearly fails to give a satisfying solution for  $\Omega(B)$  upon comparison with a numerically obtained solution. The red dashed line in Fig. 3 shows  $\Omega(B)$  calculated numerically for free spiral waves in<sup>15</sup>. The red dot-dashed line in Fig. 3 we have added for completeness. It describes the branch of unstable wave segments. At  $B = B_c \approx 0.535$  the two red branches merge in the critical finger. The

blue dotted line in Fig. 3 shows the analytical result derived by Hakim and Karma<sup>14</sup>

$$\Omega_{\text{HK}}(B) = \frac{1}{\sqrt{2}} \left( \frac{B - B_c}{K a_1} \right)^{3/2}, \quad (63)$$

which is valid close to the critical finger  $B \lesssim B_c$ . In Eq. (38)  $K \approx 0.630$  and  $B_c$  are numerically determined constants.

Although our relation for  $\Omega(B)$  is very inaccurate, it still bears some resemblance to real spirals in a certain range of frequencies. In the following we try to analyze the reasons for its failure. First of all, the analytical solution for  $\Omega(R_0)$  for the front interface yields a range of frequencies  $0.331 \lesssim \Omega \leq 1/2$  which cannot be found in numerical solutions. This range corresponds to the thin solid line in Fig. 3. The appearance of that branch is therefore due to the failure of the ansatz for the front interface in this range of frequencies. Second, the lower branch resembles wave segments which can be seen as solutions which rotate with zero frequency. However, our ansatz fails to describe solutions with small rotation frequency. The shape of the wave front  $\Theta^+(R)$  obtained from the rescaled linear eikonal equation Eq. (28) behaves in the limit  $R \rightarrow \infty$  as

$$\begin{aligned} \Theta^+(R) &= -\Omega R - \Omega \ln(R) \\ &+ \left( \Omega - \frac{1}{2\Omega} \right) \frac{1}{R} + \mathcal{O}\left(\frac{1}{R^2}\right), \quad R \rightarrow \infty. \end{aligned} \quad (64)$$

As  $B \rightarrow B_c$  and  $\Omega \rightarrow 0$ , all terms linear in  $\Omega$  vanish while the term  $\sim 1/\Omega$  grows indefinitely. Therefore, expansion Eq. (64) breaks down close to the critical finger. The correct leading order asymptotics for the critical finger reads

$$\Theta^+(R) = 2 \frac{\ln(R)}{R} + o\left(\frac{\ln(R)}{R}\right), \quad R \rightarrow \infty, \quad B = B_c. \quad (65)$$

The reason for the breakdown of the expansion Eq. (64) for  $\Omega \rightarrow 0$  is that polar coordinates are a convenient parametrization for spiral waves but a bad choice for wave segments and critical finger which are better parametrized in Cartesian coordinates. Note, that the asymptotics for  $r \rightarrow r_0$ , Eq. (32), remains valid for the critical finger and wave segments. In other words, the tip region of the critical finger and of wave segments is correctly represented by our ansatz, however, it fails in correctly predicting the whole shape of the front interface for wave segments and the critical finger.

### C. Analytical approximation for the spiral shape

Our ansatz leads to the following analytical approximation for the front and back interface of a rigidly rotating

spiral wave

$$\begin{aligned} \Theta_{\text{ans}}^\pm(R) &= -\sqrt{R^2 - R_0^2} \Omega \\ &+ \left( R_0 \Omega \pm \frac{1}{\sqrt{R_0 + 1}} \right) \arccos\left(\frac{R_0}{R}\right), \end{aligned} \quad (66)$$

where  $\Omega$  as a function of core radius  $R_0$  is given by Eq. (46). In Fig. 4 we compare the analytical prediction to numerical solutions of the dimensionless eikonal equations Eqs. (28), (29) for three given values of the rotation frequency  $\Omega$  in order to avoid the inaccuracy in the analytical relation  $\Omega(B)$ . Fig. 4 shows good agreement between theoretical and numerical results. In particular, the front interface is nicely described by the ansatz although the analytical approximation always slightly overestimates the core size. The back interface is well represented for a small core radius  $R_0$  but the agreement becomes worse for larger core radii. The reason is that the analytically predicted pulse width

$$\Delta\Theta_{\text{ans}}(R) = 2 \frac{\arccos\left(\frac{R_0}{R}\right)}{\sqrt{1 + R_0}} \quad (67)$$

displays deviations which increase for large core radii. In fact, asymptotically we find for large  $R$

$$\Delta\Theta_{\text{ans}}(R) = \frac{\pi}{\sqrt{1 + R_0}} + \mathcal{O}\left(\frac{1}{R}\right), \quad R \rightarrow \infty, \quad (68)$$

while the asymptotic behavior to the eikonal equation yields

$$\begin{aligned} \Delta\Theta(R) &= \Theta^+(R) - \Theta^-(R) \\ &= \frac{2\Omega}{B} + \mathcal{O}\left(\frac{1}{R}\right), \quad R \rightarrow \infty. \end{aligned} \quad (69)$$

If we plug the asymptotic expansion for the rotation frequency

$$\Omega = \frac{1}{R_0} + o\left(\frac{1}{R_0}\right), \quad R_0 \rightarrow \infty, \quad (70)$$

into (69) we get a different asymptotic behavior for large core radii as compared to (68). This difference explains the decreasing agreement between analytically and numerically calculated back interface with increasing  $R_0$ . Moreover, because  $B$  is intimately connected with the pulse width, it is another reason for the failure of the analytical  $\Omega$  over  $B$  relation in the vicinity of the critical finger.

The opposite limit,  $R_0 \rightarrow 0$ , implies  $\Omega \rightarrow 1/2$ ,  $B \rightarrow 1/(4\text{arcsec}(2^{1/4})) \approx 0.437171$  for the ansatz solution. This yields an Archimedean spiral

$$\lim_{R_0 \rightarrow 0} \Theta_{\text{ans}}^\pm(R) = -\frac{1}{2}(R \mp \pi), \quad (71)$$

with a back interface identical in shape to the front interface but turned by an angle  $\Delta\Theta_{\text{ans}}(R) = \pi$ . Numerically



solving the kinematic equations for zero core radius, i.e., for  $\Omega \approx 0.331$  and  $B = B_{\min} \approx 0.211$ , leads to a very similar result, compare red lines in Fig. 5 and<sup>16,22</sup>. To find even better analytical estimates for  $B$  and  $\Omega$  in the limit  $R_0 \rightarrow 0$ , we choose an Archimedean spiral with the correct leading order asymptotics as  $R \rightarrow \infty$ , i.e.

$$\Theta_{\text{ans}}^+(R) = -\Omega R, \quad (72)$$

for the front interface, and assume an identical back interface turned by an angle  $\Delta\Theta_{\text{ans}}(R) = \pi = \frac{2\Omega}{B}$ <sup>22</sup>. With this ansatz, we minimize the functional

$$\begin{aligned} S^+ &= \int_0^\infty dr (1 - K^+(r) - C_n^+(r))^2 \\ &= \frac{19}{16}\pi\Omega + \frac{4 - \pi}{2\Omega} - \log(4) - 1 \end{aligned} \quad (73)$$

with respect to  $\Omega$ . We obtain

$$S^+ = \sqrt{\frac{19}{8}(4 - \pi)\pi - 1 - \log(4)} \approx 0.144 \quad (74)$$

for

$$\Omega = \sqrt{\frac{8(4 - \pi)}{19\pi}} \approx 0.339. \quad (75)$$

The corresponding value for  $B$  is

$$B = \frac{2\Omega}{\pi} = 4\sqrt{\frac{2(4 - \pi)}{19\pi^3}} \approx 0.216. \quad (76)$$

These values, though only approximately valid, display a relative error of less than 3% when compared with the numerical results of the BCF limit. We compare this Archimedean approximation for the spiral shape with numerical solutions of the rescaled eikonal equations Eqs. (28), (29) in Fig. 5.

## V. RESULTS FOR PINNED SPIRALS

In this section we consider a pinned spiral, i. e. a wave rotating around a hole of radius  $r = r_+$  with no flux boundaries at the hole boundary. We are looking for solutions of Eqs. (21), (22) subject to the following boundary conditions

$$\theta^+(r_+) = \theta_0^+, \quad (77)$$

$$\theta^{\pm'}(r_+) = 0, \quad (78)$$

$$\theta^\pm(r) \sim r, \quad r \rightarrow \infty. \quad (79)$$

Four out of these five conditions are necessary to determine four integration constants of the ODEs. The fifth condition yields a relation between frequency  $\omega$  and hole radius  $r_+$ .

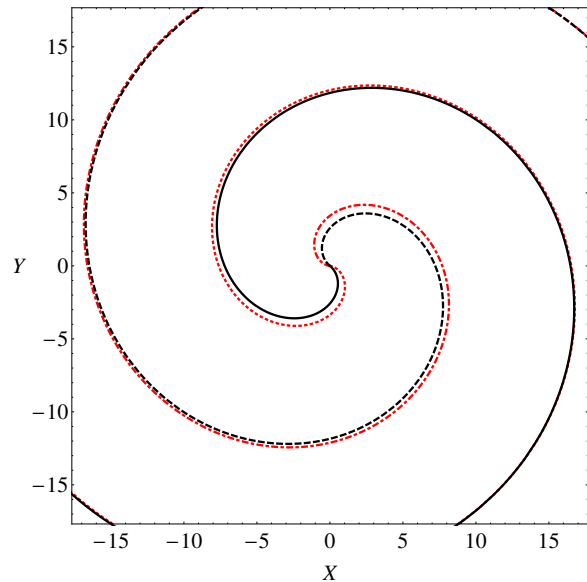


Figure 5. Spiral shape in the BCF limit of zero spiral core radius. The back interface is identical to the front interface turned by an angle  $\Delta\Theta = \pi$ . Numerical solution of the eikonal equation (red) and Archimedean approximation given by Eq. (72) (black) are plotted in such a way that they coincide far from the core. This leads to small deviations near to the center of rotation.

The front interface of a free spiral always contains a corresponding pinned spiral because the front interface displays the point  $r = r_+$  with  $\theta^{\pm'}(r_+) = 0$ . Therefore, the same ansatz Eq. (38) as was used for free spirals can be used for the front interface of a pinned spiral. Its back interface is identical in shape to the front interface but rotated by an angular puls width  $\Delta\Theta$ .

### A. Rotation frequency $\Omega$ versus hole radius $R_+$

Eliminating  $R_0$  from the  $\Omega(R_0)$  relation for free spirals, Eq. (46) by using Eq. (49), we obtain

$$\begin{aligned} R_+\Omega &= R_+\Omega \left( 1 - \frac{4\Omega^2}{(R_+\Omega - 1)^2} \right) \\ &+ \frac{\sqrt{1 - \frac{4\Omega^2}{(R_+\Omega - 1)^2}}}{\sqrt{\sqrt{R_+^2 - \frac{4\Omega^2 R_+^2}{(R_+\Omega - 1)^2}} + 1}}. \end{aligned} \quad (80)$$

Because  $R_+$  is the given hole radius, (80) already represents the desired result. Note that in contrast to free spiral waves, for a pinned spiral wave the rotation frequency does not depend on the parameter  $B$  that characterizes the strength of the interaction between wave front and back and measures the excitability of the medium. Within our approach, any dependence of the rotation frequency on  $B$  or other kinetic parameters enters through the dispersion relation for periodic pulse trains.

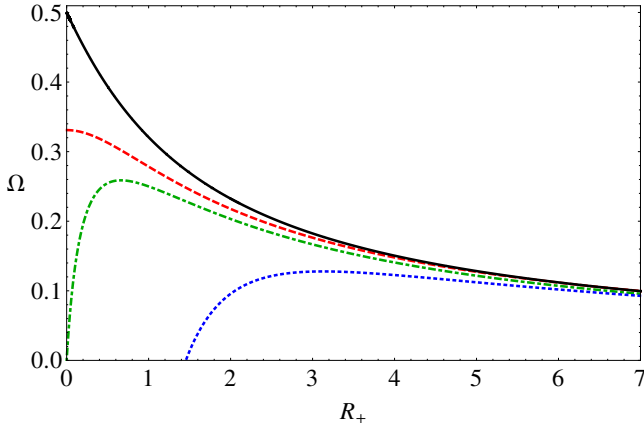


Figure 6. Rotation frequency  $\Omega$  versus hole radius  $R_+$  for spiral waves pinned to a Neumann hole. The analytical result (black solid line, Eq. (80)) is compared to Keener's result (green dot-dashed line<sup>8</sup>), the result by Hakim and Karma (blue dotted line<sup>14</sup>), and numerical solution of the linear eikonal equation (red dashed line).

As before, for small  $\epsilon$  an explicit expression can be derived perturbatively

$$\omega(r_+) = \frac{c}{r_+} - \frac{2c^{1/4}}{r_+^{7/4}}\epsilon^{3/4} + \mathcal{O}(\epsilon^{5/4}). \quad (81)$$

Eq. (81) can be compared with Keener's result<sup>8</sup>

$$\omega_K(r_+) = \frac{c(4cr_+ + \epsilon - \sqrt{\epsilon(8cr_+ + \epsilon)})}{4r_+(cr_+ + \epsilon)}, \quad (82)$$

which after expanding for small  $\epsilon$  gives

$$\omega_K(r_+) = \frac{c}{r_+} - \frac{c^{1/2}}{\sqrt{2}r_+^{3/2}}\epsilon^{1/2} + \mathcal{O}(\epsilon). \quad (83)$$

In rescaled form, Keener's result reads

$$\Omega_K(R_+) = \frac{1 + 4R_+ - \sqrt{1 + 8R_+}}{4R_+(1 + R_+)}. \quad (84)$$

Because in general the difference between the core radius  $r_0$  and the radius of the corresponding Neumann hole  $r_+$  is small, Keener's result can be applied to free spiral waves. This was done successfully by Winfree, compare<sup>6</sup>. The result obtained by Hakim and Karma<sup>14</sup> can be modified for pinned spirals according to

$$\omega_{HK}(r_+) = \frac{c}{r_+} + \frac{2^{1/3}c^{1/3}a_1}{r_+^{5/3}}\epsilon^{2/3}, \quad (85)$$

where here  $a_1 = -1.01879$  denotes the global maximum of the Airy function  $\text{Ai}(x)$ . The rescaled form of this expression

$$\Omega_{HK}(R_+) = \frac{1}{R_+} + 2^{1/3}\frac{a_1}{R_+^{5/3}}, \quad (86)$$

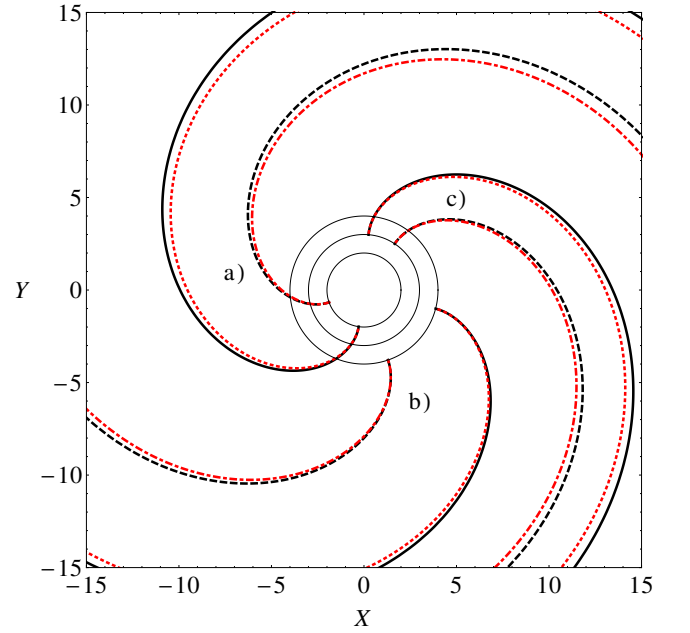


Figure 7. Shape of spiral waves pinned to a Neumann hole. Analytical result (black solid and dashed lines) and numerical results (red dotted and dot-dashed lines) are plotted for different hole radii and given excitability: a)  $R_+ = 2$ ,  $B = 0.4$ , b)  $R_+ = 4$ ,  $B = 0.3$ , c)  $R_+ = 3$ ,  $B = 0.7$ .

together with our result for  $\Omega(R_+)$  and Keener's result  $\Omega_K(R_+)$ , is compared in Fig. 6 with numerical simulations of the rescaled eikonal equations Eqs. (28), (29). All three analytical results agree well with the numerically obtained curve in the limit of large hole radius  $R_+ \rightarrow \infty$  while for small core radii  $R_+ \rightarrow 0$  partially marked deviations appear. Merely our analytical approximation produces a finite and different from zero rotation frequency for vanishing hole radius. Note the different exponents in leading order of  $\epsilon$  in the expansions Eq. (81), Eq. (83), and Eq. (85).

## B. Approximations for the wave shape $\Theta_{\text{ans}}^\pm(R)$

From the Neumann boundary condition at  $R = R_+$ , we have  $R_- = R_+$  and it follows

$$\Psi_{\text{ans}}^+(R) = \Psi_{\text{ans}}^-(R). \quad (87)$$

For the shape of the front interface we obtain

$$\Theta_{\text{ans}}^+(R) = -\Omega\sqrt{R^2 + R_+^2} \left( \frac{4\Omega^2}{(R_+\Omega - 1)^2} - 1 \right) + \frac{R_+\Omega \arccos\left(\frac{R_+}{R}\sqrt{1 - \frac{4\Omega^2}{(R_+\Omega - 1)^2}}\right)}{\sqrt{1 - \frac{4\Omega^2}{(R_+\Omega - 1)^2}}}. \quad (88)$$

The relation between hole radius  $R_+$  and rotation frequency  $\Omega$  is given by Eq. (80). Furthermore, from

the asymptotic behavior of the solutions of the rescaled eikonal equations Eqs. (28), (29) at  $R = R_+$ , we find  $\Theta^+(R_+) - \Theta^-(R_+) = \frac{2\Omega}{B}$ , from which follows

$$\Theta_{\text{ans}}^+(R) = \Theta_{\text{ans}}^-(R) + \frac{2\Omega}{B}. \quad (89)$$

We compare the analytical predictions according to Eq. (88) with numerical solutions of the kinematic equations in Fig. 7. Close to the hole, the agreement between theory and numerics is good. With larger  $R$  values, initially minor deviations arise which grow according to

$$\Theta^\pm(R) - \Theta_{\text{ans}}^\pm(R) = \gamma R + o(R), \quad R \rightarrow \infty, \quad (90)$$

where  $\gamma$  is some nonzero constant. The reason for this discrepancy is that, first, the analytical relation  $\Omega(R_+)$  is only approximately valid, and, second, the correct leading order asymptotics for the shape functions is given by  $\Theta^\pm(R) = -\Omega R + \mathcal{O}(\log(R))$ ,  $R \rightarrow \infty$ . Our ansatz reproduces only the leading order asymptotics and does not contain the logarithmic asymptotics.

## VI. CONCLUSIONS

Based on a new non-perturbative ansatz Eq. (37), we have presented analytical approximations for spiral wave solutions to the linear eikonal equation. The approximate analytical solution  $\theta_{\text{ans}}^\pm(r)$  for a rigidly rotating spiral wave displays the correct leading order asymptotic expansion of the unknown exact solution  $\theta^\pm(r)$  close to the core ( $r \rightarrow r_0$ ), at the radius of the effective Neumann hole ( $r \rightarrow r_+$ ,  $\theta^{+'}(r)$ ) and far from the core ( $r \rightarrow \infty$ ). In addition, approximate and exact solution have the same asymptotic expansion in the inflection point located on the wave back ( $r \rightarrow r_1$ ,  $\kappa(r_1) = 0$ ). The asymptotically correct treatment of these four essential regions of a spiral wave is crucial for our ansatz.

For the front interface our ansatz works quite well. In particular, the derived dependence between the rotation frequency  $\Omega$  and the core radius  $R_0$  for rigidly rotating spiral waves, Eq. (46), agrees well with numerical solutions of the linear eikonal equation. In fact, for large and intermediate core radii the agreement between theory and numerics is very close, moreover, even for small core radius our ansatz produces a more than acceptable match with the numerical results. An equally good analytical approximation for  $\Omega(R_0)$ , which is globally valid for all spiral core radii  $R_0$ , to our knowledge, does not exist. Rotation frequency and core radius are accessible in experiments with the Belousov-Zhabotinsky reaction, for example. The relation for  $\Omega(R_0)$ , Eq. (46), supplemented with the dispersion relation for one-dimensional pulse trains, can be checked in experiments.

The relation for  $\omega(r_0)$  can only be given implicitly. Using perturbation theory, it is impossible to derive a globally valid explicit approximation for  $\omega(r_0)$  starting

from Eq. (45). The reason is that the small parameter  $\epsilon$  by introducing rescaled quantities drops out of Eq. (46). This scaling gives a dominant balance. There is no scaling giving a dominant balance which leads from Eq. (45) to an equation which is simpler than Eq. (46). In other words, sooner or later we will inevitably be faced with Eq. (45) in order to obtain a globally valid solution for  $\omega(r_0)$ .

We believe that one encounters the same situation for the full free boundary approach based on the linear eikonal equations Eqs. (21), (22). They can be transformed to the rescaled eikonal equations Eqs. (28), (29) that do not contain the small parameter  $\epsilon$  any more. Within any perturbative approach to Eqs. (21), (22), which is based solely on the assumption of small  $\epsilon$ , the rescaled eikonal equations Eqs. (28), (29) must be solved. Our relatively simple analytical approximations might be a contribution to that approach.

Our ansatz gives simple analytical expressions for the shape of free spirals, Eq. (66). Not only is the region far from the core correctly represented, as it is also achieved by the Archimedean and the involute spiral, but also the tip region of a free spiral is modeled in accordance with numerical simulations of the eikonal equation. For the shape of the back interface and the dependence of the rotation frequency  $\Omega(B)$  on the excitability parameter  $B$ , the results produced by the ansatz are much less satisfactory. The reasons for the discrepancy between analytical prediction and numerical results are discussed in sections IV B and IV C.

The relatively simple  $R$ -dependence for the wave shape Eq. (66) could be the starting point for stability analysis and further analytical investigations.

In principle, one can improve the ansatz Eq. (38) by including terms involving additional constants. Higher order asymptotics at  $r_0$ ,  $r_+$ ,  $r_1$  and for  $r \rightarrow \infty$  can be taken into account to determine these constants. However, it is difficult to find terms which show the correct asymptotic behavior at one point without simultaneously destroying the correct asymptotics at other points.

## ACKNOWLEDGMENTS

We acknowledge support by the DFG via GRK 1558 (J. L.) and SFB 910 (H. E.).

## REFERENCES

- <sup>1</sup>S. Jakubith, H. H. Rotermund, W. Engel, A. von Oertzen, and G. Ertl, Phys. Rev. Lett. **65**, 3013 (1990)
- <sup>2</sup>A. Winfree, Science **175**, 634 (1972)
- <sup>3</sup>A. Zhabotinsky and A. Zaikin, J. Theor. Biology **40**, 45 (1973)
- <sup>4</sup>G. Gerisch, Naturwissenschaften **58**, 430 (1971)
- <sup>5</sup>F. Fenton, E. Cherry, H. Hastings, and S. Evans, Chaos **12**, 852 (2002)

- <sup>6</sup>A. T. Winfree, *Physica D* **49**, 125 (1991)
- <sup>7</sup>V. S. Zykov, *Simulation of wave processes in excitable media* (Manchester University Press, Manchester, 1988)
- <sup>8</sup>J. Tyson and J. Keener, *Physica D* **32**, 327 (1988)
- <sup>9</sup>V. Davydov, V. S. Zykov, and A. S. Mikhailov, *Sov. Phys. Usp.* **34**, 665 (1991)
- <sup>10</sup>A. S. Mikhailov, V. A. Davydov, and V. S. Zykov, *Physica D* **70**, 1 (1994)
- <sup>11</sup>V. S. Zykov and K. Showalter, *Phys. Rev. Lett.* **94**, 068302 (2005)
- <sup>12</sup>A. Kothe, V. S. Zykov, and H. Engel, *Phys. Rev. Lett.* **103**, 154102 (2009)
- <sup>13</sup>A. Karma, *Phys. Rev. Lett.* **66**, 2274 (1991)
- <sup>14</sup>V. Hakim and A. Karma, *Phys. Rev. E* **60**, 5073 (1999)
- <sup>15</sup>V. S. Zykov, *Phys. Rev. E* **75**, 046203 (2007)
- <sup>16</sup>V. S. Zykov, *Physica D* **238**, 931 (2009)
- <sup>17</sup>G. Bordyugov and H. Engel, *Physica D* **228**, 49 (2007)
- <sup>18</sup>W. Burton, N. Cabrera, and F. Frank, *Philos. Trans. R. Soc. London, Ser. A*, 299(1951)
- <sup>19</sup>J. Keener, *SIAM J. Appl. Math.* **46**, 1039 (1986)
- <sup>20</sup>P. Pelcé and J. Sun, *Physica D* **48**, 353 (1991)
- <sup>21</sup>C. M. Bender and S. A. Orszag, *Advanced mathematical methods for scientists and engineers* (McGraw-Hill, New York, 1978)
- <sup>22</sup>V. S. Zykov, N. Oikawa, and E. Bodenschatz, *Phys. Rev. Lett.* **107**, 254101 (2011)